

# Spin polarization in the Hubbard model with Rashba spin-orbit coupling on a ladder

José A. Riera

*Instituto de Física Rosario y Departamento de Física,  
Universidad Nacional de Rosario, Rosario, Argentina*

(Dated: March 18, 2013)

The competition between on-site Coulomb repulsion and Rashba spin-orbit coupling (RSOC) is studied on two-leg ladders by numerical techniques. By studying persistent currents in closed rings by exact diagonalization, it is found that the contribution to the current due to the RSOC  $V_{SO}$ , for a fixed value of the Hubbard repulsion  $U$  reaches a maximum at intermediate values of  $V_{SO}$ . By increasing the repulsive Hubbard coupling  $U$ , this spin-flipping current is suppressed and eventually it becomes opposite to the spin-conserving current. The main result is that the spin accumulation defined as the relative spin polarization between the two legs of the ladder is enhanced by  $U$ . Similar results for this Hubbard-Rashba model are observed for a completely different setup in which two halves of the ladders are connected to a voltage bias and the ensuing time-dependent regime is studied by the density matrix-renormalization group technique. It is also interesting a combined effect between  $V_{SO}$  and  $U$  leading to a strong enhancement of antiferromagnetic order which in turn may explain the observed behavior of the spin-flipping current. The implications of this enhancement of the spin-Hall effect with electron correlations for spintronic devices is discussed.

PACS numbers: 71.27.+a, 71.70.Ej, 73.23.-b

*Introduction.* Recent trends in the field of spintronics [1–3] exploit the possibility of controlling electron spins by purely electrical means without using magnetic materials [4], which is at the heart of the conceptual proposal of the Datta-Das spin field-effect transistor [5]. Key to this possibility is the Rashba spin-orbit (SO) interaction [6, 7] appearing due to structure inversion asymmetry of materials and which has been shown to be tuned by gate voltages in semiconductor heterostructures [8].

Although the main interest in the study of RSOC has been on its ability of generating and controlling spin polarized currents, another consequence of the interplay between charge and spin degrees of freedom induced by the RSOC is a flow of spins transversal to the flow of charge which is known as the spin-Hall effect [9–12]. If transport takes place along a planar strip, the spin-Hall effect leads to a spin accumulation with opposite projection on both edges of the strip [13, 14]. This has been experimentally observed [15, 16]. Hence, the spin-Hall effect provides a real-space separation between up and down spin electrons, like two ferromagnets with opposite polarizations, thus enhancing the metallic state and its conductance, and these features could also be employed in spintronics devices.

Since most devices and experiments about RSOC have involved semiconductors, electron correlations have mostly not been included so far in theoretical models. However, there are some systems which have been recently considered in this field where such correlations may play an important role. In the first place, RSOC has been observed in oxide heterostructures [17]. Important effects of a RSOC have been experimentally observed in other transition metal oxides, particularly the iridates where the relevant degrees of freedom are the 5d electrons on the  $\text{Ir}^{4+}$  ions, and where strong correlation effects are

expected [18]. It should be also taken into account that correlation effects become increasingly important in systems with low spatial dimensions. Interesting crossovers have been reported when moving from two-dimensional (2D) systems to quantum wires [19]. In this sense, spin-orbit effects, predominantly of the Rashba type have been studied in quantum wires [20, 21]. The presence of RSOC in graphene and carbon nanotubes has been pointed out [22] and in fact a theoretical study with up to two interacting electrons has been done on a nanotube quantum dot [23].

In this Letter, an attempt of studying the interplay between electron correlations and RSOC will be performed by considering a Hubbard model with a Rashba SOC. During the last two decades it has been realized the difficulties of tackling electron correlations theoretically. In studies of RSOC, electron correlations have been included only locally regarding quantum dots [24, 25] or on effective onedimensional (1D) systems using Tomonaga-Luttinger liquid approach [26]. For this reason, in the present Letter a two-leg ladder, which may be the narrowest quasi-1D geometry on which a spin-Hall effect could take place will be considered. The Hubbard-Rashba model on a two-leg ladder is suitable for treatment using essentially exact, unbiased, computational techniques, which have been enormously valuable in the field of strongly correlated electron systems. Particularly for mesoscopic systems, the full quantum many-body interplay between different terms of the Hamiltonian can be reliably captured. Then, the main goal is to determine and understand the behavior of the spin accumulation as a function of the RSOC and the Hubbard repulsion  $U$ . The interplay between RSOC and  $U$  with respect to a possible metal-insulator transition [27] will not be discussed in the present work.

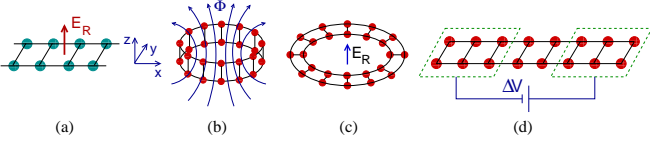


FIG. 1: (Color online) (a) The two-leg ladder system here considered; (b) a two-leg ring pierced by a magnetic flux; (c) previously study 2D rings; (d) setup used in DMRG calculations.

*Formulation.* The Hamiltonian of the Hubbard-Rashba model in a square lattice is defined as:

$$\begin{aligned}
 H = & -t_0 \sum_{\langle l,m \rangle, \sigma} (c_{l,\sigma}^\dagger c_{m,\sigma} + H.c.) + U \sum_l n_{l,\uparrow} n_{l,\downarrow} \\
 & + V_{SO} \sum_l [c_{l+\hat{x},\downarrow}^\dagger c_{l,\uparrow} - c_{l+\hat{x},\uparrow}^\dagger c_{l,\downarrow} + i(c_{l+\hat{y},\downarrow}^\dagger c_{l,\uparrow} \\
 & + c_{l+\hat{y},\uparrow}^\dagger c_{l,\downarrow}) + H.c.] \quad (1)
 \end{aligned}$$

where the notation is standard. The first two terms corresponds to the usual Hubbard model and the last term contains the RSOC [28]. The couplings  $t_0$  and  $V_{SO}$  are normalized in such a way that  $t_0^2 + V_{SO}^2 = 1$  (which is henceforth taken as the unit of energy). The longitudinal (transversal) direction of the ladder corresponds to the  $x$ -axis ( $y$ -axis), as shown in Fig. 1(a). The RSOC in (1) corresponds to an effective Rashba electric field  $E_R$  along the  $z$ -axis, i.e. perpendicular to the plane of the ladder. Open boundary conditions (OBC) are applied in the transversal direction. The total number of lattice sites is  $N = 2 \times L$ . Hamiltonian (1) corresponds to the isotropic ladder, in which couplings are the same along both directions. The present study is limited to the quarter filled system ( $n = 0.5$ ). Weak-coupling analysis [29] has shown that the Hubbard model on the isotropic ladder at  $n = 0.5$  is at the boundary between a metal (C1S0) and an insulating (C0S1) phase [30]. Exactly at the boundary, where additional metallic phases are predicted to be stable, both this study as well as numerical studies [31, 32] and the present results point to a metallic phase, even for the values of  $U > 0$  here examined. As soon as  $V_{SO}$  is turned on, the occupied bonding band will split leading to a four-point Fermi surface and the system will behave as a metal. In all cases, the length  $L$ , equal to the total number of electrons, was set equal to  $4m$  ( $m$  integer).

In order to induce persistent currents, a magnetic flux piercing the ring formed by a closed ladder has to be applied (Fig. 1(b)). This magnetic flux  $\Phi$  is included in the Hamiltonian by the usual Peierls factors, which in momentum space is equivalent to replacing  $k_x$  by  $k_x + \Phi/L$  (units in which  $e = c = \hbar = 1$  have been adopted). These Peierls factors are included in both the hopping and SO terms of (1). The resulting Hamiltonian is studied using exact diagonalization (ED) for  $U > 0$ . For the

noninteracting case,  $U = 0$ , by working in momentum space, ladders with  $L$  up to 6400 have been considered [40]. Due to the RSOC the total  $S^z$  is not conserved hence all possible values of total  $S^z$  have to be included in the Hilbert space. In order to reduce the Hilbert space dimension, translation symmetry along the longitudinal direction has been implemented thanks to the use of periodic boundary conditions (PBC) along the  $x$ -axis. Notice that the ladder ring shown in Fig. 1(b) is different from the 2D ring (Fig. 1(c)) that has been intensively studied in the non-interacting case [33–35]. Studies including Coulomb interactions for these rings have been limited to few electrons [36].

The total current is defined as  $J(\Phi) = \frac{\partial E_0(\Phi)}{\partial \Phi}$  where  $E_0(\Phi)$  is the ground state energy. The contribution from the hopping term in (1), the hopping or spin-conserving current, is then given by the usual current operator along the legs,  $\hat{j}_h = it_0 \sum_{l,\sigma} (c_{l+\hat{x},\sigma}^\dagger c_{l,\sigma} - H.c.)$ . A similar current operator can be easily derived for the contribution from the RSOC term in (1), that is, the SO or spin-flipping current,  $\hat{j}_{SO}$ . Using the Feynman-Hellmann theorem, the total current is given by  $LJ = j_h + j_{SO}$ . The spin polarization due to the spin-Hall effect is defined as  $\Delta S^z = \langle S_1^z - S_2^z \rangle / 2$ , where  $S_j^z$  is the total  $z$ -component of the spin on leg  $j$ . All physical quantities are ground state averages, and hence, they are functions of the magnetic flux  $\Phi$ . In order to determine the effects of the Rashba and Hubbard couplings on these quantities, the reasonable choice of looking at their maximum values as a function of the flux  $\Phi$  was adopted.

The second setup considered in this work is shown in Fig. 1(d), which corresponds to OBC along the  $x$ -axis. Here, at a given time the two ends of a ladder are connected to a voltage bias  $\Delta V$  generating a time-dependent regime which is studied by DMRG. Although various sophisticated approaches have been proposed within DMRG to deal with this time evolution [37–39], the simple “static” approach is implemented in the present work which is enough to reliably capture the main physical features in the small lattices studied. This is a non-equilibrium process, but a small value  $\Delta V = 0.01$  was adopted. In this case, the total current is computed as  $J(t) = \frac{\partial N_l}{\partial t}$ , where  $N_l$  is the total charge in the left half of the ladder, and  $t$  is the time measured in units of the time increment  $\Delta\tau = 0.1$ .  $J_{max}$  is computed as the average of  $J(t)$  between the first two peaks of its time evolution, which can be precisely determined with a relatively small number of retained states  $M$  within the static approach. The spin-conserving current  $j_h(t)$  was computed at the central links of the ladder.  $j_{h,max}$  was computed using the same criterion as for  $J_{max}$ .

*Results.* For the case of persistent currents, Fig. 1(b), results for the noninteracting  $U = 0$  case are shown in Fig. 2. For various lattice sizes ranging from  $L = 8$  to 6400, it can be observed the maximum values of the spin-flipping current (Fig. 2(a)) and the spin accumulation

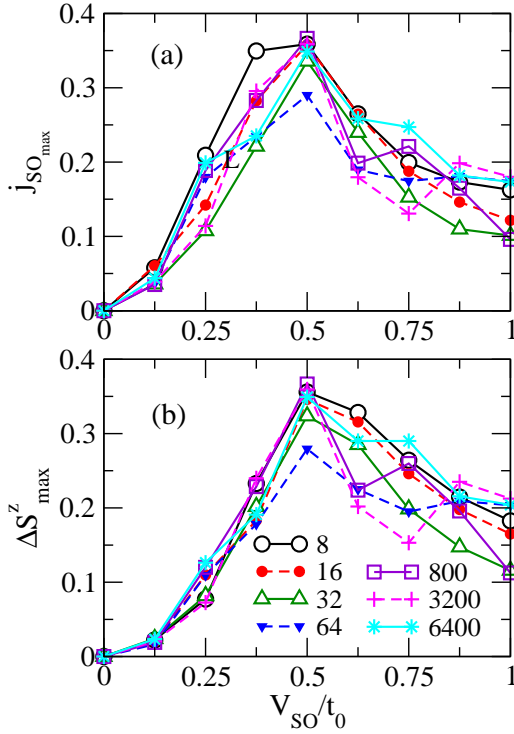


FIG. 2: (Color online) Maximum value of (a) spin-orbit current, and (b) spin accumulation  $\Delta S^z$ , as a function of  $V_{SO}/t_0$  for the noninteracting case on various two-leg ladders,  $n = 0.5$ , tight-binding calculations.

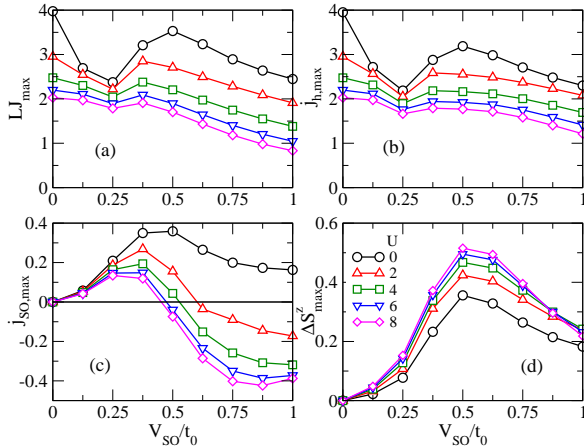


FIG. 3: (Color online) Maximum value of (a) total current, (b) hopping current, (c) spin-orbit current, and (d) spin accumulation  $\Delta S^z$  as a function of  $V_{SO}/t_0$  for various values of  $U$ . Results for the  $2 \times 8$  ladder,  $n = 0.5$ , obtained with ED.

(Fig. 2(b)) occur at  $V_{SO}/t_0 \approx 0.5$ . The curves are quite noisy due to various level crossings as a function of the flux  $\Phi$  but nonetheless the ratio  $j_{SO,max}/\Delta S^z_{max}$  follows a smooth monotonous behavior as a function of  $V_{SO}/t_0$  for large  $L$ , as shown in [40]. Taking into account this noisy behavior,  $\Delta S^z_{max}$  is quite independent of  $L$ .

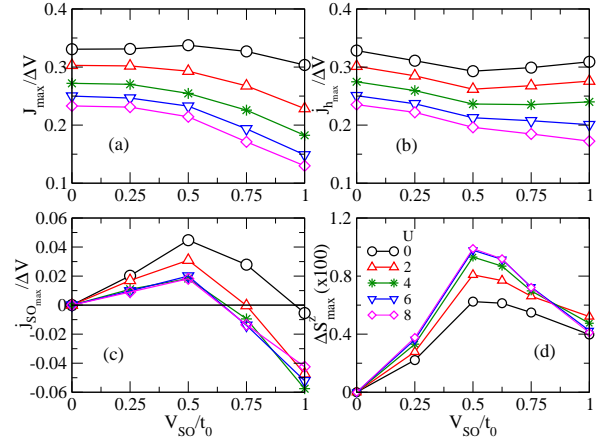


FIG. 4: (Color online) Maximum value of (a) total, (b) hopping, and (c) spin-orbit currents, divided by  $\Delta V$ , and (d) spin accumulation  $\Delta S^z$  as a function of  $V_{SO}/t_0$  for various values of  $U$ . Results for the  $2 \times 20$  ladder,  $n = 0.5$ , obtained with DMRG.

Let us discuss the correlation effects for the case of persistent currents, for  $0 \leq U \leq 8$ . Fig. 3 shows the results for the maximum values of the total current,  $I$ , the hopping and spin-orbit contributions to the current,  $j_h$  and  $j_{SO}$ , and the spin-leg polarization  $\Delta S^z$  on the  $2 \times 8$  ladder at  $n = 0.5$ . As it can be seen in Fig. 3(a), the total current for a fixed value of  $V_{SO}/t_0$  decreases with increasing  $U$ . This result is expected for  $V_{SO} = 0$ , i.e. for the pure Hubbard model, where it is well known that the conductance  $G$  decreases with increasing  $U$ , as in the one-dimensional Hubbard model presenting a Luttinger liquid behavior where  $G \sim K_\rho$  [41], as examined for ladders in [42]. The maximum value of the hopping current, shown in Fig. 3(b), follows roughly the same behavior with  $U$  and  $V_{SO}/t_0$  as the total current since it is much larger than the spin-flipping contribution. The dip in  $I$  and  $j_h$  at  $V_{SO}/t_0 \approx 0.25$  (Fig. 3(a),(b)) is just a finite size effect. On the other hand, the behavior of the maximum value of the SO current is quite interesting (Fig. 3(c)). For all values of  $U$ ,  $j_{SO,max}$  increases with  $V_{SO}/t_0$  until reaching a maximum which depends on  $U$ , and then starts to decrease becoming eventually negative, indicating that its direction is *opposed* to the hopping current, by convention. The most important results correspond to the maximum value of the spin-leg polarization shown in Fig. 3(d). One should first notice that  $\Delta S^z_{max}$  increases as a function of the Coulomb repulsion  $U$  for all values of  $V_{SO}/t_0$ . In addition, its maximum value near  $V_{SO}/t_0 = 0.5$  observed for the noninteracting case is preserved for finite  $U$ . The dependence of these properties as a function of the magnetic flux, for  $V_{SO}/t_0 = 0.5$  and 1, is shown in [40].

Results for the voltage bias setup (Fig. 1(d)), for the  $2 \times 20$  ladder, are shown in Fig. 4. The behavior of the maximum values of the total, spin-conserving and spin-flipping currents, and of the spin accumulation as a func-

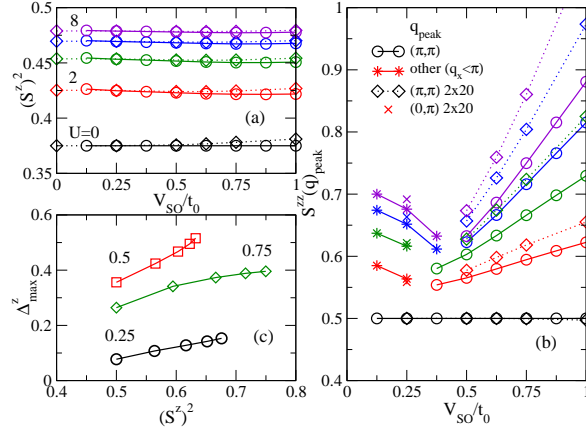


FIG. 5: (Color online) (a)  $(S^z)^2$  as a function of  $V_{SO}/t_0$  for  $U = 0, 2, 4, 6, 8$  from bottom to top for the  $2 \times 8$  ladder PBC at zero flux (circles) and for the  $2 \times 20$  ladder OBC (diamonds). (b) Peak value of the magnetic structure factor  $S^{zz}(\mathbf{q})$  as a function of  $V_{SO}/t_0$  for  $U = 0, 2, 4, 6, 8$  from bottom to top for the  $2 \times 8$  ladder PBC at zero flux (circles, stars) and for the  $2 \times 20$  ladder OBC (diamonds, crosses) if  $\mathbf{q} = (\pi, \pi)$  (other) (c) Maximum value of the spin accumulation  $\Delta S^z$  as a function of  $(S^z)^2$  at zero flux for various values of  $V_{SO}/t_0$  indicated in the plot, for the  $2 \times 8$  ladder PBC.

tion of  $V_{SO}/t_0$  for various values of  $U$ , are qualitatively strikingly similar to those shown for the setup involving persistent currents (Fig. 3) in spite of the quite different background physics involved. Notice that actually the maximum values of the currents divided by the voltage bias  $\Delta V$  are shown, which correspond to the conductance  $G$  up to a factor of  $2\pi$ . Comparison with results for the  $2 \times 16$  do not show appreciable finite-size effects. Details of the calculations are provided in [40].

Some possible explanations of the behaviors shown in Figs. 3 and 4 can be obtained by examining the dependence of various magnetic properties with the parameters  $U$  and  $V_{SO}/t_0$ . In Fig. 5(a) the average value of  $(S^z)^2$ , a measure of the magnetic moment per site [40], as a function of  $V_{SO}/t_0$  and for various values of  $U$  is shown. As expected,  $(S^z)^2$  increases with  $U$ , as it is well-known for Hubbard-like models, and it is almost independent of  $V_{SO}/t_0$ . Results for the  $2 \times 8$  ladder PBC at zero flux are virtually indistinguishable with the ones obtained for the  $2 \times 20$  ladder OBC using DMRG. More interesting are the results for the peak value of the static magnetic structure factor  $S^{zz}(\mathbf{q})$ , which are shown in Fig. 5(b) as a function of  $V_{SO}/t_0$  and for various values of  $U$ . For large values of  $V_{SO}/t_0$ ,  $S^{zz}(\mathbf{q})$  has a peak at  $\mathbf{q} = (\pi, \pi)$ , while for small values of  $V_{SO}/t_0$ ,  $S^{zz}(\mathbf{q})$  is maximal at other values of  $\mathbf{q}$ , all of them with  $q_x \neq \pi$ , and in most cases at  $\mathbf{q} = (0, \pi)$ . In the first place, as in Fig. 5(a), it is expected that  $S^{zz}(\mathbf{q})$  is enhanced by  $U$ . What is unexpected is the strong dependence of  $S^{zz}(\mathbf{q})$  with  $V_{SO}/t_0$ :  $S^{zz}(\pi, \pi)$  increases with increasing  $V_{SO}/t_0$ , and  $S^{zz}(\mathbf{q} \neq (\pi, \pi))$  increases with decreasing  $V_{SO}/t_0$ . This is a combined effect

of  $V_{SO}/t_0$  and  $U$  since for  $U = 0$ ,  $S^{zz}(\mathbf{q})$  is constant and clearly the slope of  $S^{zz}(\mathbf{q})$  with  $V_{SO}/t_0$  increases with  $U$ . Results for the  $2 \times 20$  ladder show a stronger dependence than the ones corresponding to the  $2 \times 8$  ladder and this could be explained by the fact that in DMRG  $S^{zz}(\mathbf{q})$  calculations, the only included spin-spin correlations are the ones measured from one of the central sites of the ladder.

The increase of the z-component of the magnetic moment can at least partially explain the larger values of the spin accumulation observed as a function of the Hubbard repulsion for a fixed value of  $V_{SO}/t_0$ . This is shown in Fig. 5(c) where it can be observed an almost linear dependence of  $\Delta S^z_{max}$  with  $(S^z)^2$  except for a slight upward curvature for  $V_{SO}/t_0 = 0.5$  and a slight downward curvature for  $V_{SO}/t_0 = 0.75$ . The peak of the magnetic structure factor at  $\mathbf{q} = (\pi, \pi)$ , indicating the presence of an antiferromagnetic (AFM) order could in turn provide some insight on the suppression of the spin-flipping current  $j_{SO}$  for large  $V_{SO}/t_0$  and  $U$ , shown in Figs. 3(c) and 4(c). For an AFM order, two electrons occupying nearest neighbors sites along one leg of the ladder would likely have spins with opposite projections on the  $z$ -axis. For this configuration, a spin-flipping hopping would be impossible while there would be no problem for a spin-conserving hopping (except for a cost  $U$ ). Now, once a  $t_0$ -hopping has occurred, creating a doubly-occupied site and leaving behind an empty site, a  $V_{SO}$ -hopping is now possible from the doubly-occupied site to the empty one. Hence the spin-flipping hopping takes place in a direction *opposite* to the spin-conserving one thus possibly explaining the observed change of sign of the spin-flipping current.

*Conclusions.* To summarize, we have considered perhaps the simplest system where some features associated to Rashba spin-orbit coupling can be observed [14]. This two-leg ladder system is suitable to be studied by unbiased, essentially exact, computational techniques, which allow to consider electron correlations on an equal foot with spin-conserving and spin-flipping hoppings. At quarter-filling it was observed that spin accumulation is maximal at an intermediate value of  $V_{SO}/t_0$ , independently of  $U$ . By increasing a repulsive  $U$ , the spin-flipping current is suppressed and it becomes negative for large  $V_{SO}$  and  $U$ , while spin accumulation is enhanced. These two last features can be explained by the increase of  $(S^z)^2$  and AFM correlations, the latter being a combined effect of  $V_{SO}$  and  $U$ . The present approach could be extended to wider strips which could in principle be studied by DMRG, and also by variational and diffusion Monte Carlo (plus a fixed-node approximation), and to different electron fillings. In addition, some subtle and so far controversial properties, such as spin currents, could be studied numerically on this class of strips including electron correlations. Although the present study does not include any dissipative mechanism, an enhancement of spin accumulation by electron interactions together with

a reduction of the overall current are positive features that could be taken advantage in spintronic devices.

The author wishes to acknowledge Sadamichi Maekawa for calling his attention to related problems and to George Martins for a careful reading of the manuscript. The author is supported in part by the Consejo Nacional de Investigaciones Científicas y Técnicas, Argentina.

- 
- [1] S. A. Wolf, D.D. Awschalom, R.A. Buhrman, J.M. Daughton, S. von Molnar, M.L. Roukes, A.Y. Chtchelkanova, D.M. Treger, *Science* **294**, 1488 (2001).
  - [2] G.A. Prinz, *Science* **282**, 1660 (1998).
  - [3] I. Zutic, J. Fabian, and S. Das Sarma, *Rev. Mod. Phys.* **76**, 323, (2004).
  - [4] D. Awschalom and N. Samarth, *Physics* **2**, 50 (2009).
  - [5] S. Datta, B. Das, *Appl. Phys. Lett.* **56**, 665 (1989).
  - [6] E. I. Rashba, *Sov. Phys. Solid State* **2**, 1109 (1960); Y. A. Bychkov and E. I. Rashba, *JETP Lett.* **39**, 78 (1984).
  - [7] For a review see, R. Winkler, *Spin-Orbit Coupling Effects in Two-Dimensional Electron and Hole Systems* (Springer, New York, 2003).
  - [8] J. B. Miller, D. M. Zumbuhl, C. M. Marcus, Y. B. Lyanda-Geller, D. Goldhaber-Gordon, K. Campman, and A. C. Gossard, *Phys. Rev. Lett.* **90**, 076807 (2003).
  - [9] M.I. D'yakonov, V.I. Perel, *Sov. Phys. JETP* **33**, 1053 (1971).
  - [10] J. E. Hirsch, *Phys. Rev. Lett.* **83**, 1834 (1999).
  - [11] S. Murakami, N. Nagaosa, and S.-C. Zhang, *Science* **301**, 1348 (2003).
  - [12] J. Sinova, D. Culcer, Q. Niu, N. A. Sinitsyn, T. Jungwirth, and A. H. MacDonald, *Phys. Rev. Lett.* **92**, 126603 (2004).
  - [13] B. K. Nikolić, S. Souma, L. P. Zârbo, and J. Sinova, *Phys. Rev. Lett.* **95**, 046601 (2005).
  - [14] A. G. Malshukov, L. Y. Wang, C. S. Chu, and K. A. Chao, *Phys. Rev. Lett.* **95**, 146601 (2005).
  - [15] Y. Kato, R. C. Myers, A. C. Gossard, and D. D. Awschalom, *Science* **306**, 1910 (2004).
  - [16] J. Wunderlich, B. Kaestner, J. Sinova, and T. Jungwirth, *Phys. Rev. Lett.* **94**, 047204 (2005).
  - [17] A. D. Caviglia et al., *Phys. Rev. Lett.* **104**, 126803 (2010).
  - [18] M. Trescher and E. J. Bergholtz, *Phys. Rev. B* **86**, 241111 (2012).
  - [19] P. Wenk and S. Kettemann, *Phys. Rev. B* **83**, 115301 (2011).
  - [20] C. H. L. Quay, T. L. Hughes, J. A. Sulpizio, L. N. Pfeiffer, K. W. Baldwin, K. W. West, D. Goldhaber-Gordon and R. de Picciotto, *Nature Physics* **6**, 336 (2010).
  - [21] A. E. Hansen, M. T. Bjork, C. Fasth, C. Thelander, and L. Samuelson, *Phys. Rev. B* **71**, 205328 (2005).
  - [22] D. Huertas-Hernando, F. Guinea, A. Brataas, *Phys. Rev. Lett.* **103**, 146801 (2009).
  - [23] B. Wunsch *Phys. Rev. B* **79**, 235408 (2009).
  - [24] D. F. Mross and H. Johannesson, *Phys. Rev. B* **80**, 155302 (2009).
  - [25] Q.-f. Sun, J. Wang, and H. Guo, *Phys. Rev. B* **71**, 165310 (2005).
  - [26] M. Pletyukhov, V. Gritsev, *Phys. Rev. B* **70**, 165316 (2004).
  - [27] D. A. Pesin and L. Balents, *Nature Phys.* **6**, 376 (2010).
  - [28] T. P. Pareek and P. Bruno, *Phys. Rev. B* **65**, 241305 (2002).
  - [29] L. Balents and M. P. A. Fisher, *Phys. Rev. B* **53**, 12133 (1996).
  - [30] J. Riera, D. Poilblanc, and E. Dagotto, *Eur. J. Phys. B* **7**, 53 (1999).
  - [31] R. M. Noack, S. R. White, and D. J. Scalapino, *Physica C* **270**, 281 (1996).
  - [32] M. Vojta, A. Hübsch, and R. M. Noack, *Phys. Rev. B* **63**, 045105 (2001).
  - [33] Xin Liu, M. F. Borunda, Xiong-Jun Liu, and J. Sinova, *Phys. Rev. B* **80**, 174524 (2009).
  - [34] J. S. Sheng and Kai Chang, *Phys. Rev. B* **74**, 235315 (2006).
  - [35] J. Splettstoesser, M. Governale, and U. Zulicke, *Phys. Rev. B* **68**, 165341 (2003).
  - [36] C. Daday, A. Manolescu, D. C. Marinescu, and V. Gudmundsson, *Phys. Rev. B* **84**, 115311 (2011).
  - [37] A. E. Feiguin and S.R.White, *Phys. Rev. B* **72**, 020404 (2005).
  - [38] U. Schollwöck, *Rev. Mod. Phys.* **77**, 259 (2005).
  - [39] P. Schmitteckert, *Phys. Rev. B* **70**, 121302(R), (2004).
  - [40] See Supplementary Material.
  - [41] C. L. Kane and M. P. A. Fisher, *Phys. Rev. B* **46**, 7268 (1992).
  - [42] E. Orignac and T. Giamarchi, *Phys. Rev. B* **56**, 7167 (1997).



# Supplementary material for: Spin polarization in the Hubbard model with Rashba spin-orbit coupling on a ladder

José A. Riera

Instituto de Física Rosario y Departamento de Física,  
Universidad Nacional de Rosario, Rosario, Argentina

The tight-binding part of the Hamiltonian (1) in the main text is, in momentum space:

$$H_0 = \sum_{\mathbf{k}} \begin{pmatrix} A & B & -t_{\perp} & -iV_{SO,\perp} \\ B^* & A & -iV_{SO,\perp} & -t_{\perp} \\ -t_{\perp} & iV_{SO,\perp} & A & B \\ iV_{SO,\perp} & -t_{\perp} & B^* & A \end{pmatrix} \quad (S1)$$

in the basis:  $(c_{1,\mathbf{k},\uparrow}, c_{1,\mathbf{k},\downarrow}, c_{2,\mathbf{k},\uparrow}, c_{2,\mathbf{k},\downarrow})$ , where “1”, and “2” are the two legs of the ladder.

For the general spatially anisotropic ladder:

$$\begin{aligned} A &\equiv -2t_{\parallel} \cos k_x \\ B &\equiv -2iV_{SO,\parallel} \sin k_x \end{aligned} \quad (S2)$$

In the present case,  $t_{\parallel} = t_{\perp} = t_0$ ,  $V_{SO,\parallel} = V_{SO,\perp} = V_{SO}$ .

In the tight-binding formalism, the currents  $J$ ,  $j_h$ , and  $j_{SO}$  are independently computed for each value of the magnetic flux  $\Phi$ , and hence the relation  $LJ = j_h + j_{SO}$  provides an internal check of the calculations. Similarly, in the ED and DMRG calculations,  $J$  and  $j_h$  are independently computed, hence for  $V_{SO} = 0$  the relation  $LJ = j_h$  has been checked.

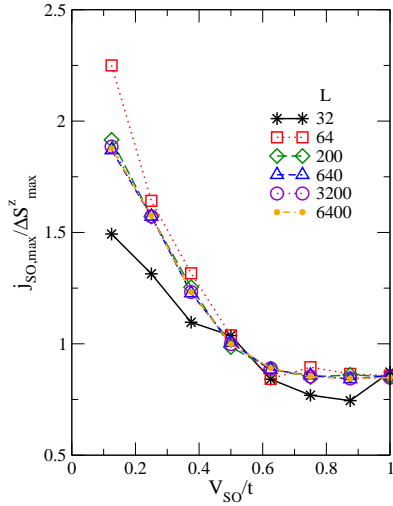


FIG. S1: Ratio of the maximum values of spin flipping current to the spin accumulation as a function of  $V_{SO}/t_0$  for the noninteracting case. Persistent currents setup. Sizes of the ladder rings are indicated in the plot.

Fig. S1 was built from data of Fig. 1 of the main text. Within numerical accuracy, there is a local minimum at  $V_{SO}/t_0 = 1$  with the value  $j_{SO}/\Delta S^z \approx 0.848$ .

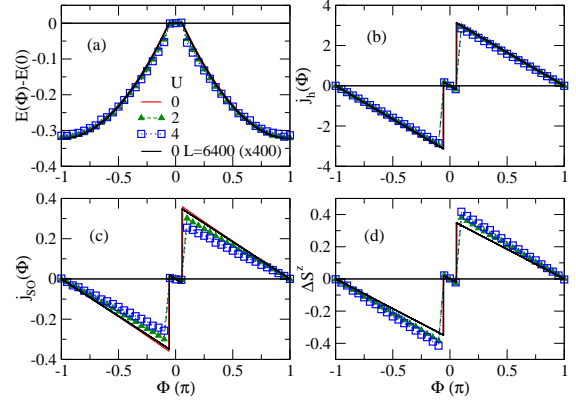


FIG. S2: (a) Ground state energy relative to the value at zero flux, (b) spin conserving current, (c) spin flipping current, and (d) spin accumulation, at  $V_{SO}/t_0 = 0.5$ , on the  $L = 8$  ladder for various values of  $U$ , and for the  $L = 6400$  ladder for the noninteracting case, as a function of the magnetic flux. The values of  $E(\Phi) - E(0)$  for  $L = 6400$  have been multiplied by 400.

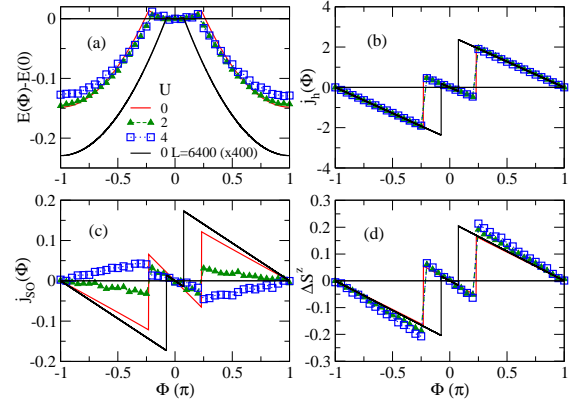


FIG. S3: Same as Fig. S2 but for  $V_{SO}/t_0 = 1$ . Notice the inversion of the spin-flipping current  $j_{SO}$  for  $U = 4$ .

In Figs. S2 and S3, the evolution of various physical properties with the magnetic flux is shown for  $V_{SO}/t_0 = 0.5$  and  $V_{SO}/t_0 = 1.0$  respectively for the  $L = 8$  ladder and various values of  $U$ . Fig. S2 shows an almost negligible difference with the results obtained for the noninteracting case with the  $L = 6400$  ladder. On the other hand, in Fig. S3 very large differences can be observed. What is remarkable in this plot is that the spin-flipping current  $j_{SO}$  (Fig. S3(c)) is inverted for  $U = 4$  thus becoming opposite to the spin-conserving current  $j_h$  (Fig. S3(b)).

In Fig. S4 some typical time evolution of the total current and of the spin accumulation are shown for various values of  $U$  and  $V_{SO}/t_0$ . It is well-known that the time evolution of the current follows an oscillatory behavior due to the interplay between kinetic and potential energies. As the number of retained states increases, or by adopting an adaptive scheme, the current reaches a

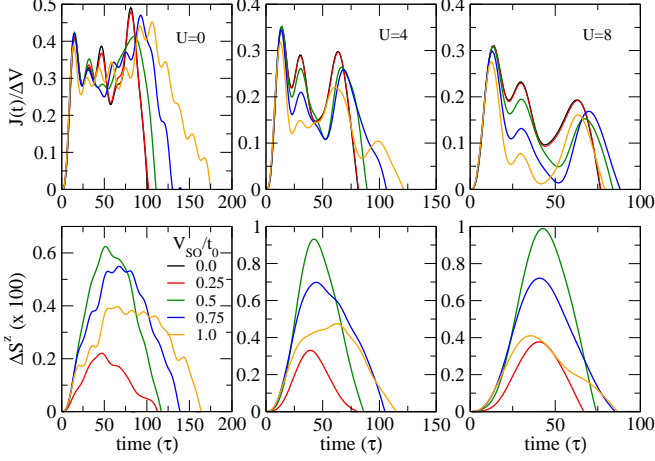


FIG. S4: Time evolution of the total current  $J$  divided by  $\Delta V$  (upper panels) and of the spin accumulation (lower panels) for  $U = 0$  (left panels),  $U = 4$  (central panels) and  $U = 8$  (right panels), and various values of  $V_{SO}/t_0$ , on the  $2 \times 20$  ladder, obtained by DMRG. Only the first half-period of the time evolution is shown, for the next half-period both  $J$  and  $\Delta S^z$  reverse their sign.

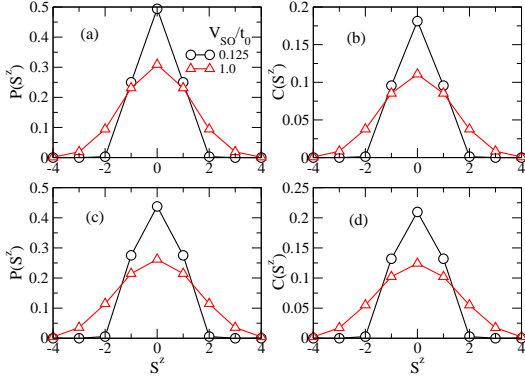


FIG. S5: (a) Weight of each  $S^z$  sector in the ground state, and (b) contribution of each  $S^z$  sector to the total average  $(S^z)^2$ , for  $U = 0$ . (c), (d), same for  $U = 8$ .

plateau during each half-period of the time evolution. The value of the current at the plateau divided by the voltage bias  $\Delta V$  is equal  $G/2\pi$ , where  $G$  is the conductance (remember that units where  $e = \hbar = 1$  were adopted). In the present case, the adopted criteria of measuring  $J_{max}$  as the average of  $J(t)$  between the first two peaks leads to a 7% overestimation of  $G$  with respect to its exact value at  $U = V_{SO} = 0$ .

$(S^z)^2$  and the static magnetic structure factor are defined as usual from the  $z - z$  spin correlations:

$$(S^z)^2 = \frac{1}{N} \sum_{j,l} \langle (S_{j,l}^z)^2 \rangle$$

$$S(\mathbf{q}) = \frac{1}{N} \sum_{\mathbf{r}_1, \mathbf{r}_2} \langle S_{\mathbf{r}_1}^z S_{\mathbf{r}_2}^z \rangle e^{i\mathbf{q} \cdot (\mathbf{r}_1 - \mathbf{r}_2)} \quad (\text{S3})$$

With this definition, is easy to find that, for the non-interacting case,  $(S^z)^2 = n_{\uparrow}(1 - n_{\downarrow}) + (\uparrow\leftrightarrow\downarrow)$ , where  $n_{\uparrow}$  ( $n_{\downarrow}$ ) is the density of electrons with  $\uparrow$  ( $\downarrow$ ) spin in a state with fixed total  $S^z$ . Note that for  $S^z = 0$ ,  $(S^z)^2 = 0.375$  which is the result shown in Fig. 5(a) of the main text, in spite of the fact that  $S^z$  is not a quantum number for the model here considered, and the ground state is a combination of subspaces with all possible  $S^z$ . Also,  $(S^z)^2 \rightarrow n = 0.5$  when  $U \rightarrow \infty$  since doubly-occupied sites become forbidden. Fig. S5 shows the weight of each  $S^z$  sector in the ground state, and the contribution of each  $S^z$  sector to the total average  $(S^z)^2$ .